

# ADR: Attention Diversification Regularization for Mitigating Overfitting in Multiple Instance Learning based Whole Slide Image Classification

Yunlong Zhang<sup>1,2</sup>, Zhongyi Shui<sup>1,2</sup>, Yunxuan Sun<sup>1,2</sup>, Honglin Li<sup>1,2</sup>, Jingxiong Li<sup>1,2</sup>, Chenglu Zhu<sup>2</sup>, Sunyi Zheng<sup>2</sup>, and Lin Yang<sup>2</sup>

<sup>1</sup> Zhejiang University

<sup>2</sup> Westlake University

**Abstract.** Multiple Instance Learning (MIL) has demonstrated effectiveness in analyzing whole slide images (WSIs), yet it often encounters overfitting challenges in real-world applications. This paper reveals the correlation between MIL’s performance and the entropy of attention values. Based on this observation, we propose Attention Diversity Regularization (ADR), a simple but effective technique aimed at promoting high entropy in attention values. Specifically, ADR introduces a negative Shannon entropy loss for attention values into the regular MIL framework. Compared to existing methods aimed at alleviating overfitting, which often necessitate additional modules or processing steps, our ADR approach requires no such extras, demonstrating simplicity and efficiency. We evaluate our ADR on three WSI classification tasks. ADR achieves superior performance over the state-of-the-art on most of them. We also show that ADR can enhance heatmaps, aligning them better with pathologists’ diagnostic criteria. The source code is available at <https://github.com/dazhangyu123/ADR>.

**Keywords:** Computational pathology · Whole slide image · Multiple instance learning · Overfitting · Entropy regularization.

## 1 Introduction

Whole slide images (WSIs) are widely recognized as the gold standard for numerous cancer diagnoses. They play a crucial role in ensuring precise diagnosis [1], prognosis [17,31], and the development of treatment plans [27]. In recent years, multiple instance learning (MIL) has emerged as a promising approach for WSI analysis [5,20,16,36,30,33,8,15,14,21]. Although considerable progress has been made on this field, recent studies have uncovered issues of overfitting in MIL due to factors like limited scale of available data [28,32,34,13], class imbalance [34], and staining bias [18,35].

There have been some recent efforts that focus on mitigating the overfitting issue from the perspectives of data augmentation [32,30,28,34] and regularization [18,13]. For data augmentation methods, DTFD-MIL [32] enlarges the number of bags by introducing the concept of pseudo-bags. Mixup-MIL [6], Remix [30],

Table 1: Detailed comparison of methods used for combating the overfitting for WSI classification. **Time** means the training time cost on CAMELYON-16 dataset. **Avg. AUC** denotes the averaged test AUC value on three datasets.

| Method           | Extra Modules/Processing   | Time            | Avg. AUC    |
|------------------|--|-----------------|-------------|
| DSMIL [13]       | Two stream architecture for critical instance and bag embeddings | 11.8 min        | 86.3        |
| DTFD-MIL [32]    |  | 12.7 min        | 90.0        |
| IBMIL [18]       | New training stage of interventional training from scratch       | 19.9 min        | 87.9        |
| MHIM-MIL [28]    | Teacher model for masking easy instances                         | 21.8 min        | 89.6        |
| <b>ADR(ours)</b> | <b>None</b>  | <b>10.5 min</b> | <b>90.8</b> |

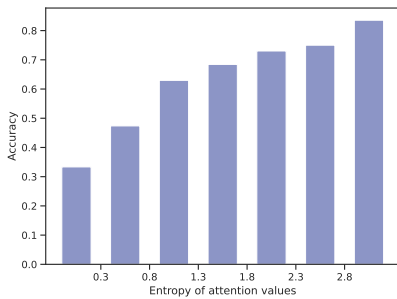


Fig. 1: Samples with higher entropy in their attention values exhibit higher accuracy. This result is obtained on the LBC dataset at seed 1.

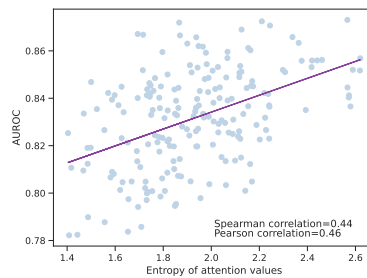


Fig. 2: There exists a moderate positive correlation between AUROC values and entropy of attention values across experimental seeds. One point denotes the outcome of a single seed on the LBC dataset.

and Slot-Mix [12] generate the pseudo bag by mixing two bags. WENO [22], MHIM-MIL [28], and STKIM [34] create hard bags/samples by masking the easy instances in the bag. For the regularization methods, DSMIL [13], H<sup>2</sup>MIL [9], and DAS-MIL [2] consider the hierarchical structure of patches and aggregate multi-scale representations in attention mechanisms. Some studies introduce self-attention layers [24] and graph neural networks [7,3,29] to model correlations between different areas. Although these methods achieve promising results, the majority of them introduce intricate modules/processing (refer to Tab. 1 second column), which not only significantly increase computational time but also limit their scalability.

In this paper, we reveal that the *entropy of attention values* is closely linked to MIL’s performance. In Fig. 1, we observe that samples with higher entropy in their attention values tend to demonstrate higher accuracy. Fig. 2 illustrates the moderate positive correlation between AUROC and entropy of attention values across experimental seeds. Leveraging these insights, we propose Attention Diversification Regularization (ADR), a straightforward yet effective method to address overfitting. This regularization only requires plugging a negative entropy

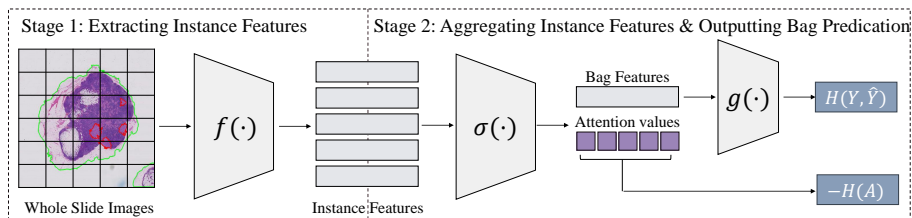


Fig. 3: Overview of plugging ADR into MIL framework. ADR adds only a negative entropy regularization for attention values to the regular MIL framework.

loss for attention values to the regular MIL paradigm (see Fig. 3). A preliminary comparison between our ADR and existing methods is shown in Table 1. Our ADR stands out from existing methods by not requiring any additional modules or processing, while also imposing minimal computational overhead, highlighting its simplicity and efficiency. Our experimental evaluations on three benchmark datasets (CAMELYON16, CAMELYON17, and our in-house LBC dataset) demonstrate the superior performance of our proposed method. Additionally, we show that ADR enhances heatmaps, aligning them more closely with pathologists’ diagnostic criteria.

## 2 Method

We present ADR, a plug-and-play regularization to enhance the MIL framework, building upon the commonly used MIL framework, ABMIL [10]. Sec. 2.1 provides a brief overview of ABMIL for WSI classification. In Sec. 2.2, we present ADR and then integrate it into ABMIL. Fig. 3 depicts the overview of our solution. Sec. 2.3 consolidates various approaches aimed at mitigating overfitting from the aspect of excessive concentration of attention values.

### 2.1 ABMIL for WSI Analysis

For the WSI classification problem, we have access to the WSI  $\mathbf{X}$  along with its slide-level label  $\mathbf{Y}$ . Typically, the resolution of a WSI ranges from  $50,000 \times 50,000$  to  $100,000 \times 100,000$ , making it computationally infeasible to be directly used for training. To resolve this, regular MIL framework, represented by ABMIL [10], segments full resolution WSIs into non-overlapping patches  $\{\mathbf{x}_n\}_{n=1}^N$ , following applying a two-step process to predict the slide label  $\hat{\mathbf{Y}}$ . Next, we provide a detailed introduction to these two steps.

**Extracting instance feature.** In the original paper, ABMIL utilizes an Imagenet pre-trained encoder to extract instance features. However, recent research [19,4] has shown that replacing this encoder with one pre-trained using SSL can lead to significant performance improvements. Hence, following [34], we employ the ViT-S/16 pre-trained on 36,666 WSIs [11] as our encoder.

**Aggregating instance features and outputting bag predication.** ABMIL aggregates all instance embeddings into the bag embedding using a gated attention operator, which can be written as:

$$\mathbf{z} = \sum_{n=1}^N a_n \mathbf{h}_n, \quad (1)$$

where  $a_n = \sigma(\mathbf{h}_n)$  represents the attention values for  $n$ -th instance,  $\mathbf{h}_n$ . Specifically, the gated attention mechanism  $\sigma(\mathbf{h}_n)$  can be formulated as:

$$\sigma(\mathbf{h}_n) = \frac{\exp\{\mathbf{w}^T(\tanh(\mathbf{V}_1 \mathbf{h}_n) \odot \text{sigm}(\mathbf{V}_2 \mathbf{h}_n))\}}{\sum_{j=1}^N \exp\{\mathbf{w}^T(\tanh(\mathbf{V}_1 \mathbf{h}_j) \odot \text{sigm}(\mathbf{V}_2 \mathbf{h}_j))\}}, \quad (2)$$

where  $\mathbf{V}_1, \mathbf{V}_2 \in \mathbb{R}^{L \times M}$ ,  $\mathbf{w} \in \mathbb{R}^{L \times 1}$  are parameters,  $\odot$  is an element-wise multiplication and  $\text{sigm}(\cdot)$  is the sigmoid non-linearity. Obtaining the bag embedding, ABMIL outputs the bag prediction by suspending a MLP layer  $\hat{\mathbf{Y}} = g(\mathbf{z})$ . The loss for training the ABMIL is defined as:

$$L_{ce} = H(\mathbf{Y}, \hat{\mathbf{Y}}) = - \sum_i \mathbf{Y}_i \log \hat{\mathbf{Y}}_i \quad (3)$$

## 2.2 Attention Diversification Regularization

The objective of ADR is to maximize the entropy  $H(A)$  of attention values,  $A = \{a_n\}_{n=1}^N$ . This is achieved by formulating ADR as the negative Shannon entropy [23]:

$$L_{adr} = -H(A) = - \sum_n a_n \log a_n \quad (4)$$

This formulation aims to prevent attention values from being concentrated on minority instances. By combining Eq. 3 and 4, the final objective of our solution can be formulated as:

$$L_{total} = L_{ce} + \lambda L_{adr} \quad (5)$$

where  $\lambda$  is a hyperparameter that balances the trade-off between  $L_{ce}$  and  $L_{adr}$ .

**Discussion.** ADR serves a similar role to the KL-divergence loss in the C2C [25] by assigning attention values to more patches. However, there are distinct differences between them. Firstly, while ADR operates on all instances, the KL-divergence loss in C2C focuses on instances within a cluster. Secondly, the KL-divergence loss forces the attention mechanism to weigh all instances uniformly, whereas the negative Shannon entropy prevents attention values from concentrating solely on a few instances. This disparity makes the KL-divergence loss unsuitable as our objective (validated in Sec. 3).

### 2.3 Relation to Existing Works

In this section, we relate our ADR and several recent efforts through their impact on suppressing attention value concentration. This can improve the understanding for our method as well as these methods.

**Excessive concentration of attention values.** Several existing studies [13,34] have revealed that attention values in ABMIL tend to concentrate on a small number of instances, compared with the tumor regions outlined by pathologists. A recent study [34] has revealed that the excessive concentration of attention values will cause the overfitting of attention mechanism.

**Understanding existing methods and ADR from mitigating excessive concentration of attention values.** Several existing methods as well as our ADR alleviate overfitting by mitigating the excessive concentration of attention values. Masking-based methods [22,28,34] mask out the instances with the highest attention values, allocating their attention values to remaining instances. Clustering-based methods [25,7] group instances into clusters and randomly sample instances from these clusters, ensuring attention values are not overly focused on minority instances. MBA [34] generates the heatmap by averaging the attention values generated by multiple attention layers, thereby avoiding the over-concentration of attention values. In contrast, our ADR approach directly applies regularization to disperse attention values, thereby addressing concentration directly.

## 3 Experiments

**Datasets and Evaluation Metrics.** The performance of ADR is evaluated on two public WSI datasets, i.e., CAMELYON16 [1] and CAMELYON17 [1], and one private dataset, LBC. CAMELYON16 dataset consists of 400 WSIs in total, including 270 for training and 130 for testing. Following [32,13,34], we further randomly split the training and validation sets from the official training set with a ratio of 9:1. CAMELYON17 dataset contains 1,000 WSIs collected from five hospitals, categorized into different slide labels such as Normal, isolated tumor cells, Micro-metastases, and Macro-metastases. Due to the absence of labels for the test set, the training set (500 WSIs) is reallocated to validate the OOD performance. Specifically, 200 WSIs from the fourth and fifth hospitals are designated as the test set, while the remaining 300 WSIs are randomly split for training and validation in a 9:1 ratio. The liquid-based cytology (LBC) dataset collected 1,989 WSIs and included 4 classes, i.e., Negative, ASC-US, LSIL, and ASC-H/HSIL. We randomly split the whole dataset into training, validation, and test sets with the ratio of 6:2:2. Following [15,34], macro-AUC and macro-F1 scores are reported. Each main experiment is conducted five times with random parameter initializations, and the average classification performance and standard deviation are reported. Besides, following [19,32,34], the test performance is reported in epochs with the best validation performance.

**Implementation Details.** (1) *Pre-processing.* We follow the pre-processing of CLAM [19], which involves threshold segmentation and filtering to locate tissue

Table 2: The performance of different MIL approaches across three datasets and two evaluation metrics. The most superior performance is highlighted in **bold**.

| Method        | CAMELYON-16        |                    | CAMELYON-17        |                    | LBC                |                    |
|---------------|--------------------|--------------------|--------------------|--------------------|--------------------|--------------------|
|               | F1-score           | AUC                | F1-score           | AUC                | F1-score           | AUC                |
| Max-pooling   | 0.903±0.054        | 0.956±0.029        | 0.413±0.077        | 0.722±0.069        | 0.590±0.043        | 0.829±0.023        |
| Mean-pooling  | 0.577±0.057        | 0.569±0.081        | 0.402±0.026        | 0.751±0.015        | 0.559±0.024        | 0.827±0.012        |
| Clam-SB [19]  | 0.925±0.035        | 0.969±0.024        | 0.523±0.020        | 0.846±0.020        | 0.617±0.022        | 0.865±0.018        |
| LossAttn [26] | 0.908±0.031        | 0.928±0.014        | 0.575±0.051        | 0.865±0.016        | 0.621±0.012        | 0.843±0.006        |
| ABMIL [10]    | 0.914±0.031        | 0.945±0.027        | 0.522±0.050        | 0.853±0.016        | 0.595±0.036        | 0.831±0.022        |
| TransMIL [24] | 0.922±0.019        | 0.943±0.009        | 0.554±0.048        | 0.792±0.029        | 0.539±0.028        | 0.805±0.010        |
| DSMIL [13]    | 0.943±0.007        | 0.966±0.009        | 0.532±0.064        | 0.804±0.032        | 0.562±0.028        | 0.820±0.033        |
| DTFD-MIL [32] | 0.948±0.007        | <b>0.980±0.011</b> | 0.535±0.046        | 0.877±0.018        | 0.612±0.034        | 0.842±0.010        |
| IBMIL [18]    | 0.912±0.034        | 0.954±0.022        | 0.557±0.034        | 0.850±0.024        | 0.604±0.032        | 0.834±0.014        |
| MHIM-MIL [28] | 0.932±0.024        | 0.970±0.037        | 0.541±0.022        | 0.845±0.026        | 0.658±0.041        | 0.872±0.022        |
| ILRA [29]     | 0.904±0.071        | 0.940±0.060        | 0.631±0.051        | 0.860±0.020        | 0.618±0.051        | 0.859±0.017        |
| ADR(ours)     | <b>0.951±0.004</b> | 0.967±0.008        | <b>0.638±0.007</b> | <b>0.883±0.013</b> | <b>0.664±0.021</b> | <b>0.874±0.012</b> |

regions in each WSI. From these regions, we extract non-overlapping patches of size  $256 \times 256$  at a magnification of  $\times 20$ . (2) *Model Architecture*. Learnable components of the model include one fully-connected layer to reduce features to 128 dimensions, a gated attention network, and a fully-connected layer for making predictions. (3) *Optimization*. The model is trained for 50 epochs using a cosine learning rate decay starting at 0.0001. We employ an Adam optimizer with a weight decay of 0.0001, and the batch size is set to 1. (4) *Hyperparameters*. The default  $\lambda$  is set as 0.01, 0.1, and 0.1 for CAMELYON16, CAMELYON17, and LBC, respectively.

**Performance comparison with SOTA methods.** We mainly compare with attention-based MIL methods including AB-MIL [10], DSMIL [13], CLAM-SB [19], TransMIL [24], DTFD-MIL [32], IBMIL [18], MHIM-MIL [28], ILRA [29] and LossAttn [26]. In addition, we compared two traditional MIL pooling operations, Max-pooling and Mean-pooling. The results of all other methods are reproduced using the official code they provide under the same settings. As presented in Tab. 2, our ADR achieves the best performance on five out of six metric terms. Particularly noteworthy is its performance on the CAMELYON17 and LBC datasets, which are more complex than the CAMELYON16 dataset due to a higher number of classes and more imbalanced class ratios. Despite these challenges, our ADR consistently achieves the best performance across all four metric terms for both datasets.

**Performance comparison of integrating our ADR into different MIL methods.** To illustrate the versatility of our ADR in enhancing the performance of various MIL methods, we choose three commonly used MIL frameworks, AB-MIL [10], MHA [34], and LossAttn [26], as baseline methods. Fig. 4 shows the performance comparison with and without our proposed ADR. The plots consistently show improvements in AUC across different datasets, underscoring the effectiveness of ADR in enhancing the performance of diverse MIL frameworks.

**Ablation.** We conducted an ablation analysis on the CAMELYON17 dataset to examine the individual contributions of ADR. We varied the weight of ADR,  $\lambda$ ,

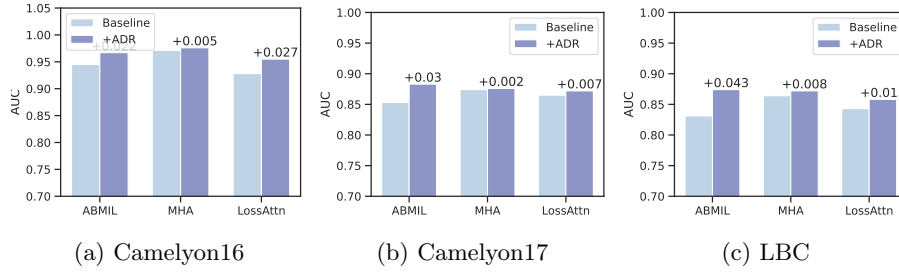


Fig. 4: Performance comparison before and after plugging our ADR into three MIL methods, ABMIL, MHA, and LossAttn. ADR consistently improves their performance across three datasets, as indicated by the comparison between the light blue and dark blue bars.

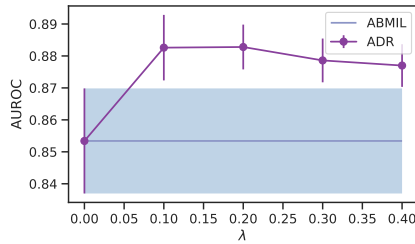


Fig. 5: Ablation results on the CAMELYON17 dataset. Choosing an appropriate  $\lambda$  is critical for ADR.

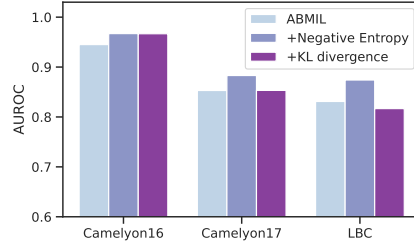


Fig. 6: Performance comparison of using negative entropy and KL divergence as the loss formulation of ADR.

across a range of values:  $\{0, 0.1, 0.2, 0.3, 0.4\}$ . Here,  $\lambda = 0$  indicates the exclusion of ADR. As depicted in Fig. 5, setting  $\lambda > 0$  consistently enhances performance compared to the baseline ( $\lambda = 0$ ). However, performance begins to degrade with larger  $\lambda$  values. Thus, selecting an appropriate  $\lambda$  is crucial for optimizing the effectiveness of ADR.

#### Negative entropy V.S. KL divergence as the loss formulation of ADR.

To compare their difference as the loss formulation for ADR, we compare AUROC results across three datasets. Fig. 6 presents the performance of ABMIL, ABMIL with negative entropy, and ABMIL with KL divergence. We find that negative entropy yields comparable performance to KL divergence on CAMELYON16 and notably outperforms KL divergence on the other two datasets. Additionally, KL divergence leads to performance degradation on the LBC dataset, indicating its unsuitability for the ADR formulation.

**Heatmap Visualization.** The heatmap can identify important instances that provide insight into the prediction. In clinical practice, the heatmap is always used to ensure the reliability of the method by comparing it with expert knowledge and serve as an indicator for the automatic selection of regions of interest

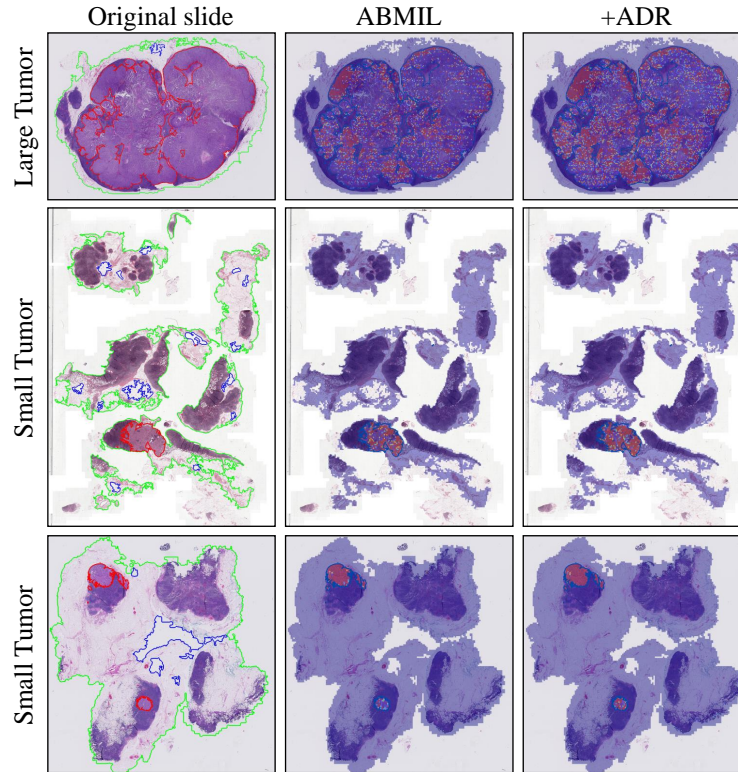


Fig. 7: Heatmap visualization of WSIs produced by ABMIL and ADR (Zoom-in for best view). We selected three WSIs from the CAMELYON16 dataset: one slide with large tumor regions and two slides with small tumor regions. ADR assigns attention values to a broader range of tumor instances compared to ABMIL, leading to better alignment with expert annotations.

[27]. Fig. 7 presents heatmap visualizations illustrating three examples of our ADR compared to the baseline method, ABMIL [10].

In the first whole slide image (WSI), a large tumor region is present. Contrasting with ABMIL, ADR disperses attention across a broader range of tumor instances. Moving to the second and third WSIs, which contain smaller tumor regions, ABMIL concentrates solely on a part of tumor instances, whereas ADR effectively identifies the entire tumor region.

## 4 Conclusion

Our experiments on three datasets highlight the efficacy of ADR in addressing overfitting challenges within the MIL framework. Compared with existing solutions, the simplicity of ADR is worth reemphasizing. It requires no additional

modules or processing, involving only one hyperparameter,  $\lambda$ . In practice, users only need to select an appropriate  $\lambda$  for their specific dataset when implementing ADR. Moreover, the effectiveness of data augmentation techniques [32,30,28,34] have been extensively validated. Intuitively, these techniques are complementary to our ADR. The combination of these two techniques is a future work.

## References

1. Bejnordi, B.E., Veta, M., Van Diest, P.J., Van Ginneken, B., Karssemeijer, N., Litjens, G., Van Der Laak, J.A., Hermsen, M., Manson, Q.F., Balkenhol, M., et al.: Diagnostic assessment of deep learning algorithms for detection of lymph node metastases in women with breast cancer. *Jama* **318**(22), 2199–2210 (2017)
2. Bontempo, G., Bolelli, F., Porrello, A., Calderara, S., Ficarra, E.: A graph-based multi-scale approach with knowledge distillation for wsi classification. *TMI* (2023)
3. Chan, T.H., Cendra, F.J., Ma, L., Yin, G., Yu, L.: Histopathology whole slide image analysis with heterogeneous graph representation learning. In: *CVPR2023*
4. Dehaene, O., Camara, A., Moindrot, O., de Lavergne, A., Courtiol, P.: Self-supervision closes the gap between weak and strong supervision in histology. *arXiv preprint arXiv:2012.03583* (2020)
5. Ding, S., Wang, J., Li, J., Shi, J.: Multi-scale prototypical transformer for whole slide image classification. In: *MICCAI*. pp. 602–611. Springer (2023)
6. Gadermayr, M., Koller, L., Tschuchnig, M., Stangassinger, L.M., Kreutzer, C., Couillard-Despres, S., Oostingh, G.J., Hittmair, A.: Mixup-mil: Novel data augmentation for multiple instance learning and a study on thyroid cancer diagnosis. In: *MICCAI*. pp. 477–486. Springer (2023)
7. Guan, Y., Zhang, J., Tian, K., Yang, S., Dong, P., Xiang, J., Yang, W., Huang, J., Zhang, Y., Han, X.: Node-aligned graph convolutional network for whole-slide image representation and classification. In: *CVPR*. pp. 18813–18823 (2022)
8. Guo, Z., Zhao, W., Wang, S., Yu, L.: Higt: Hierarchical interaction graph-transformer for whole slide image analysis. In: *MICCAI2023*
9. Hou, W., Yu, L., Lin, C., Huang, H., Yu, R., Qin, J., Wang, L.:  $H^2$ -mil: Exploring hierarchical representation with heterogeneous multiple instance learning for whole slide image analysis. In: *AAAI*. vol. 36, pp. 933–941 (2022)
10. Ilse, M., Tomczak, J., Welling, M.: Attention-based deep multiple instance learning. In: *ICML*. pp. 2127–2136. PMLR (2018)
11. Kang, M., Song, H., Park, S., Yoo, D., Pereira, S.: Benchmarking self-supervised learning on diverse pathology datasets. In: *CVPR*. pp. 3344–3354 (2023)
12. Keum, S., Kim, S., Lee, S., Lee, J.: Slot-mixup with subsampling: A simple regularization for wsi classification. *arXiv preprint arXiv:2311.17466* (2023)
13. Li, B., Li, Y., Eliceiri, K.W.: Dual-stream multiple instance learning network for whole slide image classification with self-supervised contrastive learning. In: *CVPR*. pp. 14318–14328 (2021)
14. Li, H., Zhang, Y., Zhu, C., Cai, J., Zheng, S., Yang, L.: Long-mil: Scaling long contextual multiple instance learning for histopathology whole slide image analysis. *arXiv preprint arXiv:2311.12885* (2023)
15. Li, H., Zhu, C., Zhang, Y., Sun, Y., Shui, Z., Kuang, W., Zheng, S., Yang, L.: Task-specific fine-tuning via variational information bottleneck for weakly-supervised pathology whole slide image classification. In: *CVPR*. pp. 7454–7463 (2023)

16. Li, J., Chen, W., Huang, X., Yang, S., Hu, Z., Duan, Q., Metaxas, D.N., Li, H., Zhang, S.: Hybrid supervision learning for pathology whole slide image classification. In: MICCAI. pp. 309–318. Springer (2021)
17. Li, R., Yao, J., Zhu, X., Li, Y., Huang, J.: Graph cnn for survival analysis on whole slide pathological images. In: MICCAI. pp. 174–182. Springer (2018)
18. Lin, T., Yu, Z., Hu, H., Xu, Y., Chen, C.W.: Interventional bag multi-instance learning on whole-slide pathological images. In: CVPR. pp. 19830–19839 (2023)
19. Lu, M.Y., Williamson, D.F., Chen, T.Y., Chen, R.J., Barbieri, M., Mahmood, F.: Data-efficient and weakly supervised computational pathology on whole-slide images. *Nature biomedical engineering* **5**(6), 555–570 (2021)
20. Myronenko, A., Xu, Z., Yang, D., Roth, H.R., Xu, D.: Accounting for dependencies in deep learning based multiple instance learning for whole slide imaging. In: MICCAI. pp. 329–338. Springer (2021)
21. Qu, L., Luo, X., Liu, S., Wang, M., Song, Z.: Dgmil: Distribution guided multiple instance learning for whole slide image classification. In: MICCAI2022
22. Qu, L., Wang, M., Song, Z., et al.: Bi-directional weakly supervised knowledge distillation for whole slide image classification. *Neurips* **35**, 15368–15381 (2022)
23. Shannon, C.E.: A mathematical theory of communication. *The Bell system technical journal* **27**(3), 379–423 (1948)
24. Shao, Z., Bian, H., Chen, Y., Wang, Y., Zhang, J., Ji, X., et al.: Transmil: Transformer based correlated multiple instance learning for whole slide image classification. *Neurips* **34**, 2136–2147 (2021)
25. Sharma, Y., Shrivastava, A., Ehsan, L., Moskaluk, C.A., Syed, S., Brown, D.: Cluster-to-conquer: A framework for end-to-end multi-instance learning for whole slide image classification. In: MIDL. pp. 682–698. PMLR (2021)
26. Shi, X., Xing, F., Xie, Y., Zhang, Z., Cui, L., Yang, L.: In: AAAI. vol. 34, pp. 5742–5749 (2020)
27. Song, A.H., Jaume, G., Williamson, D.F., Lu, M.Y., Vaidya, A., Miller, T.R., Mahmood, F.: Artificial intelligence for digital and computational pathology. *Nature Reviews Bioengineering* **1**(12), 930–949 (2023)
28. Tang, W., Huang, S., Zhang, X., Zhou, F., Zhang, Y., Liu, B.: Multiple instance learning framework with masked hard instance mining for whole slide image classification. *arXiv preprint arXiv:2307.15254* (2023)
29. Xiang, J., Zhang, J.: Exploring low-rank property in multiple instance learning for whole slide image classification. In: ICLR (2022)
30. Yang, J., Chen, H., Zhao, Y., Yang, F., Zhang, Y., He, L., Yao, J.: Remix: A general and efficient framework for multiple instance learning based whole slide image classification. In: MICCAI. pp. 35–45. Springer (2022)
31. Yao, J., Zhu, X., Jonnagaddala, J., Hawkins, N., Huang, J.: Whole slide images based cancer survival prediction using attention guided deep multiple instance learning networks. *MIA* **65**, 101789 (2020)
32. Zhang, H., Meng, Y., Zhao, Y., Qiao, Y., Yang, X., Coupland, S.E., Zheng, Y.: Dtdf-mil: Double-tier feature distillation multiple instance learning for histopathology whole slide image classification. In: CVPR. pp. 18802–18812 (2022)
33. Zhang, J., Zhang, X., Ma, K., Gupta, R., Saltz, J., Vakalopoulou, M., Samaras, D.: Gigapixel whole-slide images classification using locally supervised learning. In: MICCAI. pp. 192–201. Springer (2022)
34. Zhang, Y., Li, H., Sun, Y., Zheng, S., Zhu, C., Yang, L.: Attention-challenging multiple instance learning for whole slide image classification. *arXiv preprint arXiv:2311.07125* (2023)

35. Zhang, Y., Sun, Y., Li, H., Zheng, S., Zhu, C., Yang, L.: Benchmarking the robustness of deep neural networks to common corruptions in digital pathology. In: MICCAI. pp. 242–252. Springer (2022)
36. Zheng, Y., Li, J., Shi, J., Xie, F., Jiang, Z.: Kernel attention transformer (kat) for histopathology whole slide image classification. In: MICCAI2022